

# Constraining large scale HI bias using redshifted 21-cm signal from the post-reionization epoch

Tapomoy Guha Sarkar<sup>1\*</sup>, Sourav Mitra<sup>1†</sup>, Suman Majumdar<sup>2,3‡</sup>

Tirthankar Roy Choudhury<sup>1§</sup>

<sup>1</sup>Harish-Chandra Research Institute, Chhatnag Road, Jhusi, Allahabad, 211019 India.

<sup>2</sup>Department of Physics & Meteorology, IIT, Kharagpur 721302, India.

<sup>3</sup>Centre for Theoretical Studies, IIT, Kharagpur 721302, India.

14 November 2018

## ABSTRACT

In the absence of complex astrophysical processes that characterize the reionization era, the 21-cm emission from neutral hydrogen (HI) in the post-reionization epoch is believed to be an excellent tracer of the underlying dark matter distribution. Assuming a background cosmology, it is modelled through (i) a bias function  $b(k, z)$ , which relates HI to the dark matter distribution and (ii) a mean neutral fraction ( $\bar{x}_{\text{HI}}$ ) which sets its amplitude. In this paper, we investigate the nature of large scale HI bias. The post-reionization HI is modelled using gravity only N-Body simulations and a suitable prescription for assigning gas to the dark matter halos. Using the simulated bias as the fiducial model for HI distribution at  $z \leq 4$ , we have generated a hypothetical data set for the 21-cm angular power spectrum ( $C_\ell$ ) using a noise model based on parameters of an extended version of the GMRT. The binned  $C_\ell$  is assumed to be measured with  $\text{SNR} \gtrsim 4$  in the range  $400 \leq \ell \leq 8000$  at a fiducial redshift  $z = 2.5$ . We explore the possibility of constraining  $b(k)$  using the Principal Component Analysis (PCA) on this simulated data. Our analysis shows that in the range  $0.2 < k < 2 \text{ Mpc}^{-1}$ , the simulated data set cannot distinguish between models exhibiting different  $k$  dependences, provided  $1 \lesssim b(k) \lesssim 2$  which sets the  $2\text{-}\sigma$  limits. This justifies the use of linear bias model on large scales. The largely uncertain  $\bar{x}_{\text{HI}}$  is treated as a free parameter resulting in degradation of the bias reconstruction. The given simulated data is found to constrain the fiducial  $\bar{x}_{\text{HI}}$  with an accuracy of  $\sim 4\%$  ( $2\text{-}\sigma$  error). The method outlined here, could be successfully implemented on future observational data sets to constrain  $b(k, z)$  and  $\bar{x}_{\text{HI}}$  and thereby enhance our understanding of the low redshift Universe.

**Key words:** cosmology: theory – large-scale structure of Universe - cosmology: diffuse radiation

## 1 INTRODUCTION

Following the epoch of reionization ( $z \sim 6$ ), the low density gas gets completely ionized (Becker, Fan & White 2001; Fan, Carilli & Keating 2006). However, a small fraction of neutral hydrogen (HI) survives, and is confined to the over-dense regions of the IGM. At this redshifts the bulk of the neutral gas is contained in clouds with column density greater than  $2 \times 10^{20} \text{ atoms/cm}^2$ . Observations indicate that these regions can be identified as Damped Ly- $\alpha$  (DLA) systems (Wolfe, Gawiser & Prochaska 2005), which are self-shielded from further ionization and house  $\sim 80\%$  of the HI at  $1 < z < 4$ . In this redshift range the neutral fraction remains

constant with  $\Omega_{\text{HI}} \sim 0.001$  (Lanzetta, Wolfe & Turnshek 1995; Storrie-Lombardi, McMahon & Irwin 1996; Rao & Turnshek 2000; Péroux et al. 2003).

The distribution and clustering properties of DLAs suggest that they are associated with galaxies, which represent highly non-linear matter over densities (Haehnelt, Steinmetz & Rauch 2000). These clumped HI regions saturate the Gunn-Peterson optical depth (Gunn & Peterson 1965) and hence cannot be probed using Ly- $\alpha$  absorption. They are, however the dominant source for the 21-cm radiation. In the post reionization epoch, Ly- $\alpha$  scattering and the Wouthuysen-Field coupling (Wouthuysen 1952; Purcell & Field 1956; Furlanetto, Oh & Briggs 2006) increases the population of the hyperfine triplet state of HI. This makes the spin temperature  $T_s$  much greater than the CMB temperature  $T_\gamma$ , whereby the 21-cm radiation is seen in emission (Madau, Meiksin & Rees 1997; Bharadwaj & Ali 2004; Loeb & Zaldarriaga 2004). The 21-cm flux from individual HI

\* E-mail: tapomoy@hri.res.in

† E-mail: smitra@hri.res.in

‡ E-mail: sumanm@phy.iitkgp.ernet.in

§ E-mail: tirth@hri.res.in

clouds is too weak ( $< 10\mu\text{Jy}$ ) for detection in radio observations with existing facilities, unless the effect of gravitational lensing by intervening matter enhances the image of the clouds significantly (Saini, Bharadwaj & Sethi 2001). The redshifted 21-cm signal however forms a diffuse background in all radio observations at  $z < 6$  (frequencies  $> 203$  MHz). Several radio telescopes, like the presently functioning GMRT<sup>1</sup>, and future instruments MWA<sup>2</sup> and SKA<sup>3</sup> aim to detect this weak cosmological signal submerged in large astrophysical foregrounds (Santos, Cooray & Knox 2005; McQuinn et al. 2006; Ali, Bharadwaj & Chengalur 2008).

The study of large scale structures in redshift surveys and numerical simulations reveal that the galaxies (for that matter any non linear structure) trace the underlying dark matter distribution with a possible bias (Mo & White 1996; Dekel & Lahav 1999). Associating the post-reionization HI with dark matter halos implies that the gas traces the underlying dark matter distribution with a possible bias function  $b(k) = [P_{\text{HI}}(k)/P(k)]^{1/2}$ , where  $P_{\text{HI}}(k)$  and  $P(k)$  denote the power spectra of HI and dark matter density fluctuations respectively. This function is believed to quantify the clustering property of the neutral gas. It is believed that on small scales (below the Jean's length), the bias is a scale dependent function. However, it is reasonably scale-independent on large scales (Fang et al. 1993). Further, the bias depends on the redshift. The use of the post-reionization 21-cm signal (Bharadwaj & Sethi 2001; Bharadwaj, Nath & Sethi 2001; Wyithe & Loeb 2007; Loeb & Wyithe 2008; Wyithe & Loeb 2008; Visbal, Loeb & Wyithe 2009) as a tracer of dark matter opens up new avenues towards various cosmological investigations (Wyithe, Loeb & Geil 2007; Chang et al. 2008; Bharadwaj, Sethi & Saini 2009; Mao et al. 2008) and cross-correlation studies (Guha Sarkar, Datta & Bharadwaj 2009; Guha Sarkar 2010; Guha Sarkar et al. 2011). The underlying bias model is crucial while forecasting or interpreting some of these results.

In this paper we have investigated the nature of HI bias in the post-reionization epoch. The HI fluctuations are simulated at redshifts  $z < 6$  and HI bias is obtained at various redshifts from the simulated dark matter and HI power spectra. This is similar to the earlier work by Bagla, Khandai & Datta (2010) and Marín et al. (2010). The simulated bias function is assumed to be our fiducial model for HI distribution at low redshifts. We have studied the feasibility of constraining this fiducial model with observed data. Here we have focused on the multi frequency angular power spectrum (MAPS) (Datta, Choudhury & Bharadwaj 2007)–measurable directly from observed radio data and dependent on the bias model. Assuming a standard cosmological model and a known dark matter power spectrum we have used the Principal Component Analysis (PCA) on simulated MAPS data for a hypothetical radio-interferometric experiment to put constraints on the bias model. The method is similar to the one used for power spectrum estimation using the CMB data (Efstathiou & Bond 1999; Hu & Holder 2003; Leach 2006) and constraining reionization (Mitra, Choudhury & Ferrara 2011; Mitra, Choudhury & Ferrara 2012). Stringent constraints on the bias function with future data sets would be crucial in modelling the distribution of neutral gas at low redshifts and justify the use of HI as a tracer of the underlying dark matter field. This would be

useful for both analytical and numerical work involving the post-reionization HI distribution.

The paper is organized as follows – in the next section we discuss the simulation of HI distribution and the general features of the bias function. Following that, we discuss the HI multi-frequency angular power spectrum (MAPS), a statistical quantifier directly measurable from radio-interferometric experiments. Finally we use the principal component analysis to investigate the possibility of constraining the bias model with simulated MAPS (Datta, Choudhury & Bharadwaj 2007) data.

## 2 SIMULATION RESULTS - THE BIAS MODEL

We have obtained the dark matter distribution using the PM N-body code developed by Bharadwaj & Srikant (2004), assuming a fiducial cosmological model (used throughout the paper)  $\Omega_m = 0.2726$ ,  $\Omega_\Lambda = 0.726$ ,  $\Omega_b = 0.0456$ ,  $h = 0.705$ ,  $T_{\text{cmb}} = 2.728\text{K}$ ,  $\sigma_8 = 0.809$ ,  $n_s = 0.96$  (all parameters from WMAP 7 year data (Komatsu & et al. 2011; Jarosik & et al. 2011)). We simulate  $608^3$  particles in  $1216^3$  grids with grid spacing 0.1 Mpc in a  $121.6\text{Mpc}^3$  box. The mass assigned to each dark matter particle is  $m_{\text{part}} = 2.12 \times 10^8 M_\odot h^{-1}$ . The initial particle distribution and velocity field generated using Zel'dovich approximation (at  $z \sim 25$ ) are evolved only under gravity. The particle position and velocities are then obtained as output at different redshifts  $1.5 \leq z \leq 4$  at intervals of  $\delta z = 0.5$ . We have used the Friends-of-Friends algorithm (Davis et al. 1985) to identify dark matter over-densities as halos, taking linking length  $b = 0.2$  (in units of mean inter-particle distance). This gives a reasonably good match with the theoretical halo mass function (Jenkins et al. 2001; Sheth & Tormen 2002) for masses as small as  $= 10m_{\text{part}}$ . The halo mass function obtained from simulation is found to be in excellent agreement with the Sheth-Tormen mass function in the mass range  $10^9 \leq M \leq 10^{13} h^{-1} M_\odot$ .

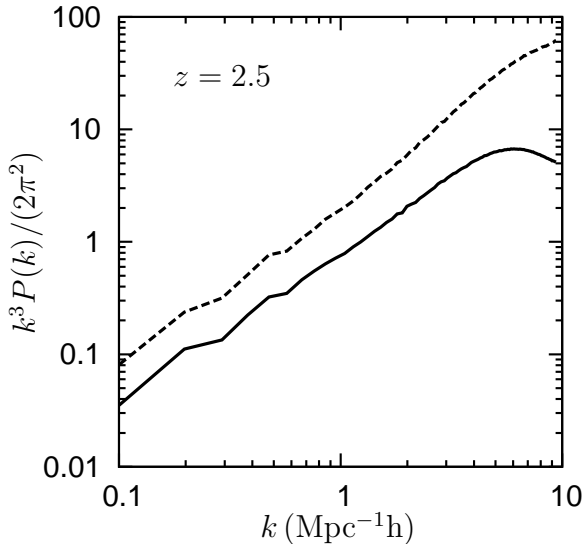
We follow the prescription of Bagla, Khandai & Datta (2010), to populate the halos with neutral hydrogen and thereby identify them as DLAs. Equation (3) of Bagla, Khandai & Datta (2010) relates the virial mass of halos,  $M$  with its circular velocity  $v_{\text{circ}}$ . The neutral gas in halos can self shield itself from ionizing radiation only if the circular velocity is above a threshold of  $v_{\text{circ}} = 30\text{km/sec}$  at  $z \sim 3$ . This sets a lower cutoff for the halo mass  $M_{\text{min}}$ . Further, halos are populated with gas in a way, such that the very massive halos do not contain any HI. An upper cut-off scale to halo mass  $M_{\text{max}}$  is chosen using  $v_{\text{circ}} = 200\text{km/sec}$ , above which we do not assign any HI to halos. This is consistent with the observation that very massive halos do not contain any gas in neutral form (Pontzen et al. 2008). The total neutral gas is then distributed such that the mass of the gas assigned is proportional to the mass of the halo between these two cut-off limits. We note that there is nothing canonical about this scheme. However, with the basic physical picture in the background this is the simplest model. Results obtained using alternative HI assignment schemes are not expected to be drastically different (Bagla, Khandai & Datta 2010).

Figure 1 shows the simulated power spectra of dark matter and HI distribution at a fiducial redshift  $z = 2.5$ . The dark matter power spectrum is seen to be consistent with the transfer function given by Eisenstein & Hu (1998) and the scale invariant primordial power spectrum (Harrison 1970; Zeldovich 1972). The HI power spectrum has a greater amplitude than its dark matter counterpart in the entire  $k$ -range allowed by the simulation parameters. Figure 2 shows the behaviour of the bias function  $b(k, z)$ . We have

<sup>1</sup> <http://www.gmrt.ncra.tifr.res.in/>

<sup>2</sup> <http://www.mwatelescope.org/>

<sup>3</sup> <http://www.skatelescope.org/>



**Figure 1.** The simulated power spectra for dark matter distribution (solid line) and the HI density field (dashed line) at redshift  $z = 2.5$ .

obtained the scale dependence of the HI bias for various redshifts in the range  $1.5 \leq z \leq 4$ . At these redshifts, the bias is seen to be greater than unity, a feature that is observed in the clustering of high redshift galaxies (Mo & White 1996; Wyithe & Brown 2009). On large cosmological scales the bias remains constant and grows monotonically at small scales, where non-linear effects are at play. This is a generic feature seen at all redshifts. The  $k$ -range over which the bias function remains scale independent is larger at the lower redshifts. The linear bias model is hence seen to hold reasonably well on large scales. The scale dependence of bias for a given redshift is fitted using a cubic polynomial with parameters summarized in Table 1. The inset in Figure 2 shows the redshift dependence of the linear bias which indicates a monotonic increase. This is also consistent with the expected  $z$ -dependence of high redshift galaxy bias. The behaviour of the linear bias for small  $k$ -values as a function of redshift is non-linear and can be fitted by an approximate power law of the form  $\sim z^2$ . This scaling relationship of bias with  $z$  is found to be sensitive to the mass resolution of the simulation. The similar dependence of HI bias with  $k$  and  $z$  has been observed earlier by Bagla, Khandai & Datta (2010) with a computationally robust Tree N-body code. Here we show that, the same generic features and similar scaling relations for bias can be obtained by using a simpler and computationally less expensive PM N-body code. Our aim is to use this scale and redshift dependence of bias, obtained from our simulation as the fiducial model for the post reionization HI distribution. We shall subsequently investigate the feasibility of constraining this model using Principal Component Analysis (PCA) on simulated MAPS data.

### 3 HI 21-CM ANGULAR POWER SPECTRUM - SIMULATED DATA

Redshifted 21-cm observations have an unique advantage over other cosmological probes since it maps the 3D density field and gives a tomographic image of the Universe. In this paper we have quantified the statistical properties of the fluctuations in the redshifted 21-cm brightness temperature  $T(\hat{\mathbf{n}}, z)$  on the sky is quantified through the multi frequency angular power spectrum MAPS, defined as  $C_\ell(\Delta z) = \langle a_{\ell m}(z) a_{\ell m}^*(z + \Delta z) \rangle$ , where

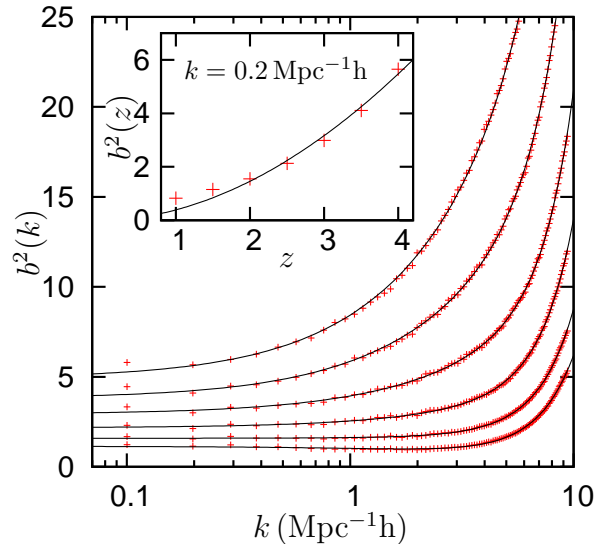


**Figure 2.** The simulated bias function for  $z = 1.5, 2.0, 2.5, 3.0, 3.5$  and  $4.0$  (bottom to top) showing the scale dependence. The inset shows the variation of the large-scale linear bias as a function of redshift.

$z$	$c_3$	$c_2$	$c_1$	$c_0$
1.5	0.0029	0.0365	-0.1561	1.1402
2.0	0.0052	0.0177	0.0176	1.5837
2.5	0.0101	-0.0245	0.3951	2.1672
3.0	0.0160	-0.0884	1.0835	2.9287
3.5	0.0234	-0.1537	2.1854	3.8050
4.0	0.0248	-0.1655	3.6684	4.9061

**Table 1.** The fit parameters for bias function of the form  $b^2(k) = c_3 k^3 + c_2 k^2 + c_1 k + c_0$  for various redshifts  $1.5 \leq z \leq 4.0$ .

$a_{\ell m}(z) = \int d\Omega_{\hat{\mathbf{n}}} Y_{\ell m}^*(\hat{\mathbf{n}}) T(\hat{\mathbf{n}}, z)$ . This measures the correlation of the spherical harmonic components of the temperature field at two redshift slices separated by  $\Delta z$ . In the flat-sky approximation and incorporating the redshift space distortion effect we have (Datta, Choudhury & Bharadwaj 2007)

$$C_\ell = \frac{\bar{T}^2}{\pi r^2} \int_0^\infty dk_{\parallel} \cos(k_{\parallel} \Delta r) P_{\text{HI}}^s(\mathbf{k}) \quad (1)$$

for correlation between HI at comoving distances  $r$  and  $r + \Delta r$ ,  $\bar{T} = 4\text{mK}(1+z)^2 \left( \frac{\Omega_b h^2}{0.02} \right) \frac{H_0}{H(z)} \left( \frac{0.7}{h} \right)$ ,  $k = \sqrt{\left( \frac{\ell}{r} \right)^2 + k_{\parallel}^2}$  and  $P_{\text{HI}}^s$  denotes the redshift space HI power spectrum given by

$$P_{\text{HI}}^s(\mathbf{k}) = \bar{x}_{\text{HI}}^2 b^2(k, z) D_+^2 \left[ 1 + \beta \left( \frac{k_{\parallel}}{k} \right)^2 \right]^2 P(k) \quad (2)$$

where the mean neutral fraction  $\bar{x}_{\text{HI}}$  is assumed to have a fiducial value  $2.45 \times 10^{-2}$ ,  $\beta = f/b(k, z)$ ,  $f = d \ln D_+ / d \ln a$  where,  $D_+$  represents the growing mode of density perturbations,  $a$  is the cosmological scale factor and  $P(k)$  denotes the present day matter power spectrum.

We use MAPS as an alternative to the more commonly used 3D power spectrum since it has a few features that makes its measurement more convenient. Firstly we note that as a function of  $\ell$  (angular scales) and  $\Delta z$  (radial separations) the MAPS encapsulate the entire three dimensional information regarding the HI distribution. In this approach, the fluctuations in the transverse di-

rection are Fourier transformed, while the radial direction is kept unchanged in the real frequency space. No cosmological information is however lost. Secondly, 21-cm signal is deeply submerged in astrophysical foregrounds. These foregrounds are known to have a smooth and slow variation with frequency, whereas the signal is more localized along the frequency axis. The distinct spectral ( $\Delta z$ ) behaviour has been proposed to be an useful method to separate the cosmological signal from foreground contaminants. In fact it has been shown that foregrounds can be completely removed by subtracting out a suitable polynomial in  $\Delta\nu$  from  $C_\ell(\Delta\nu)$  (Ghosh et al. 2011). It is hence advantageous to use MAPS which maintains the difference between the frequency and angular information in an observation. The 3D power spectrum on the contrary mixes up frequency and transverse information through the full 3D Fourier transform. Further, for a large band width radio observation, covering large radial separations light cone effect is expected to affect the signal. This can also be easily incorporated into MAPS unlike the 3D power spectrum which mixes up the information from different time slices. The key advantage, however, in using the angular power spectrum is that it can be obtained directly from radio data. The quantity of interest in radio-interferometric experiments is the complex Visibility  $\mathcal{V}(\mathbf{U}, \nu)$  measured for a pair of antennas separated by a distance  $\mathbf{d}$  as a function of baseline  $\mathbf{U} = \mathbf{d}/\lambda$  and frequency  $\nu$ . The method of Visibility correlation to estimate the angular power spectrum has been well established (Bharadwaj & Sethi 2001; Bharadwaj & Ali 2005). This follows from the fact that  $\langle \mathcal{V}(\mathbf{U}, \nu) \mathcal{V}^*(\mathbf{U}, \nu + \Delta\nu) \rangle \propto C_\ell(\Delta\nu)$ . Here the angular multipole  $\ell$  is identified with the baseline  $U$  as  $\ell = 2\pi U$  and one has assumed that the antenna primary beam is either de-convolved or is sufficiently peaked so that it maybe treated as a Dirac delta function. Further the constant of proportionality takes care of the units and depends on the various telescope parameters.

The angular power spectrum at a multipole  $\ell$  is obtained by projecting the 3D power spectrum. The integral in Equation 1, sums over the modes whose projection on the plane of the sky is  $\ell/r$ . Hence,  $C_\ell$  has contributions from matter power spectrum only for  $k > \ell/r$ . The shape of  $C_\ell$  is dictated by the matter power spectrum  $P(k)$  and the bias  $b(k)$ . The amplitude depends on quantities dependent on the background cosmological model as well as the astrophysical properties of the IGM. We emphasize here that, the mean neutral fraction and the HI bias are the only two non-cosmological parameters in our model for the HI distribution at low redshifts. Predicting the nature of  $C_\ell$  in a given cosmological paradigm is then crucially dependent on the underlying bias model and the value of the neutral fraction.

The  $\Delta\nu$  dependance of the MAPS  $C_\ell(\Delta\nu)$  measures the correlation between the various 2D modes as a function of radial separation  $\Delta r$  ( $\Delta\nu$ ). The signal is seen to decorrelate for large radial separations, the decorrelation being faster for larger  $\ell$  values. For a given  $\ell$ , one gets independent estimates of  $C_\ell$  for radial separations greater than the correlation length. Projection of the 3D power spectrum leads the availability of fewer Fourier modes. However, for a given band width  $B$ , one may combine the signals emanating from epechs separated by the correlation length  $\Delta\nu_C$  in the radial direction. Noting that the amplitude of the signal does not change significantly over the radial separation corresponding to the band width, one has  $\sim B/\Delta\nu_c$  independent measurements of  $C_\ell(\Delta z = 0)$ . We have adopted the simplified picture where the noise in  $C_\ell(\Delta z = 0)$  gets reduced owing to the combination of these  $B/\Delta\nu_c$  realizations. A more complete analysis would incor-

porate the correlation for  $\Delta\nu < \Delta\nu_c$ . We plan to take this up in a future work.

Figure 3 shows the 3D HI power spectrum at the fiducial redshift  $z = 2.5$  obtained using the dark matter power spectrum of Eisenstein & Hu (1998). We have used the WMAP 7 year cosmological model throughout. Figure 4 shows the corresponding HI angular power spectrum. The shape of  $C_\ell$  is dictated by the shape of the matter power spectrum, the bias function, and the background cosmological model. The amplitude is set by various quantities that depend on the cosmological model and the growth of linear perturbations. The global mean neutral fraction also appears in the amplitude and plays a crucial role in determining the mean level for 21-cm emission. Hence, for a fixed cosmological model, the bias and the neutral fraction, solely determine the fluctuations of the post-reionization HI density field. We have used the bias model obtained from numerical simulations in the last section to evaluate the  $C_\ell$ . We assume that the binned angular power spectrum is measured at seven  $\ell$  bins – the data being generated using Equation 1 using the fiducial bias model.

The noise estimates are presented using the formalism used by Mao et al. (2008) for the 3D power spectrum and Bharadwaj & Ali (2005) and Bagla, Khandai & Datta (2010) for the angular power spectrum. We have used hypothetical telescope parameters for these estimates. We consider radio telescope with 60 GMRT like antennae (diameter 45 m) distributed randomly over a region  $1\text{km} \times 1\text{km}$ . We assume  $T_{sys} \sim 100K$ . We consider a radio-observation at frequency  $\nu = 405\text{MHz}$  with a bandwidth  $B = 32\text{MHz}$  for an observation time of 1000 hrs.

In order to attain desired sensitivities we have assumed that the data is binned whereby several nearby  $\ell$ - modes are combined to increase the SNR. Further, in the radial direction, the signal is assumed to decorrelate for  $\Delta\nu > 0.5\text{MHz}$ , so that we have 64 independent measurements of  $C_\ell$  for the given band width of 32MHz. The 7- $\ell$  bins chosen here allows the binned power spectrum to be measured at a  $\text{SNR} \gtrsim 4$  in the entire range  $400 \leq \ell \leq 8000$ . One would ideally expect to measure the power spectrum at a large number of  $\ell$  values which would necessarily compromise the obtained sensitivities. With the given set of observational parameters, one may, in principle choose a finer binning. It shall however degrade the SNR below the level of detectability. Choosing arbitrarily fine  $\ell$ - bins and simultaneously maintaining the same SNR would require improved observational parameters which may be unreasonable if not impossible. The same reasoning applies to noise estimation for the 3D power spectrum where for a given set of observational parameters, the choice of  $k$ - bins is dictated by the requirement of sensitivity. In the figure 3, showing the 3D power spectrum a  $4 - \sigma$  detection of  $P_{\text{HI}}(k)$  in the central bin requires the full  $k$ - range to be divided into 18 equal logarithmic bins for the same observational parameters.

The noise in  $C_\ell$  and  $P_{\text{HI}}(k)$  is dominated by cosmic variance at small  $\ell/k$  (large scales), whereas, instrumental noise dominates at large  $\ell/k$  values (small scales). We point out that the error estimates predicted for a hypothetical observation are based on reasonable telescope parameters and future observations are expected to reflect similar sensitivities.

We note here that several crucial observational difficulties hinder  $C_\ell$  to be measured at a high SNR. Separating the astrophysical foregrounds, which are several order larger in magnitude than the signal is a major challenge (Santos, Cooray & Knox 2005; McQuinn et al. 2006; Ali, Bharadwaj & Chengalur 2008; Ghosh et al. 2010; Ghosh et al. 2011). Several methods have been suggested for the removal of foregrounds most of which

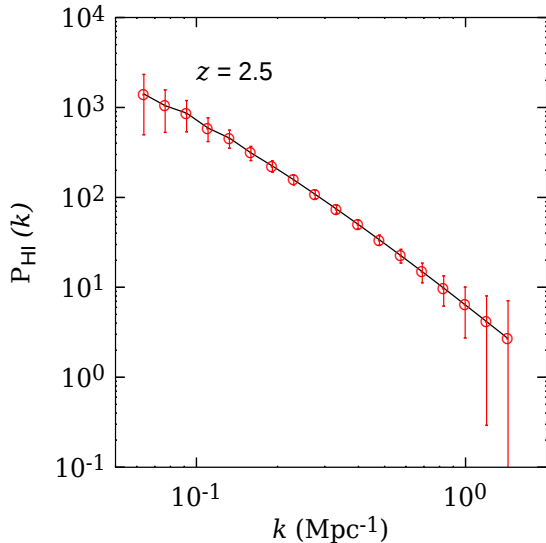


**Figure 3.** The theoretical 3D HI power spectrum  $P_{\text{HI}}^s(k)$  for  $z = 2.5$  as a function of  $k$ , at  $\mu = 0.5$ . The points with  $2\text{-}\sigma$  error-bars represent the hypothetical binned data.

uses the distinct spectral property of the 21 cm signal as against that of the foreground contaminants. The multi frequency angular power spectrum (MAPS)  $C_\ell(\Delta\nu)$  is itself useful for this purpose (Ghosh et al. 2010; Ghosh et al. 2011). Whereas this signal  $C_\ell(\Delta\nu)$  decorrelates over large  $\Delta\nu$ , the foregrounds remain correlated – a feature that maybe used to separate the two. In our subsequent discussions we assume that the foregrounds have been removed. As mentioned earlier, the angular power spectrum can directly be measured from raw visibility data. One requires to incorporate the primary beam of the antenna in establishing this connection (Bharadwaj & Ali 2005). In this paper we assume that such difficulties are overcome and the angular power spectrum is measured with sufficiently high SNR.

In the next section we use the  $C_\ell$  data generated with these assumptions to perform the PCA. If the 3D HI power spectrum is measured at some  $(k, \mu)$  it would be possible to determine the bias directly from a knowledge of the dark matter power spectrum. The bias would be measured at the  $k$ -values where the data is available. The results for the 3D analysis is summarized in section 5.

#### 4 PRINCIPAL COMPONENT ANALYSIS

In this section, we discuss the principal component method towards constraining the bias function using  $C_\ell$  data. We consider a set of  $n_{\text{obs}}$  observational data points labeled by  $\mathcal{C}_{\ell_{\text{obs}}}$  where  $\ell_{\text{obs}}$  runs over the different  $\ell$  values for which  $C_\ell$  is obtained (Fig. 4).

In our attempt to reconstruct  $b(k)$  in the range  $[k_{\text{min}}, k_{\text{max}}]$ , we assume that the bias which is an unknown function of  $k$ , can be represented by a set of  $n_{\text{bin}}$  discrete free parameters  $b_i = b(k_i)$  where the entire  $k$ -range is binned such that  $k_i$  corresponds to the  $i^{\text{th}}$  bin of width given by

$$\Delta \ln k_i = \frac{\ln k_{\text{max}} - \ln k_{\text{min}}}{n_{\text{bin}} - 1} \quad (3)$$

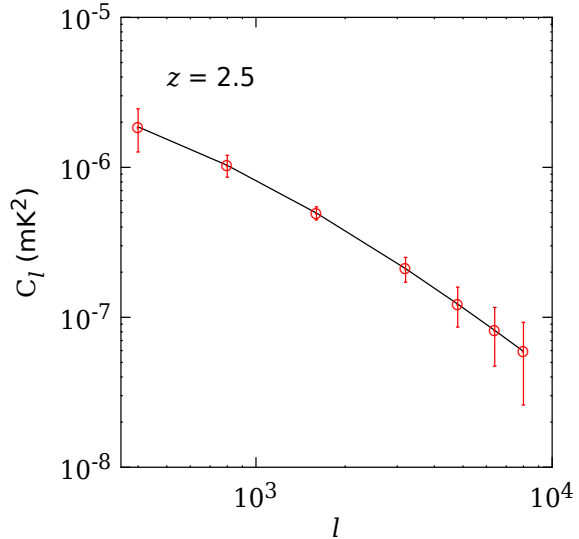


**Figure 4.** The theoretical angular power spectrum  $C_\ell$  for  $z = 2.5$  as a function of a  $\ell$ . The points with  $2\text{-}\sigma$  error-bars represent the hypothetical data.

We have chosen  $n_{\text{bin}} = 61$  and a  $k$ -range  $0.13 \leq k \leq 5.3 \text{ Mpc}^{-1}$ . Our choice is dictated by the fact that for  $k < 0.13 \text{ Mpc}^{-1}$ , the  $C_\ell$  corresponding to the smallest  $\ell$  is insensitive to  $b(k)$  and for  $k > 5.3 \text{ Mpc}^{-1}$  there is no data probing those scales. This truncation is also justified as the Fisher information matrix, we shall see, tends to zero beyond this  $k$ -range.

The Fisher matrix is constructed as

$$F_{ij} = \sum_{\ell_{\text{obs}}} \frac{1}{\sigma_{\ell_{\text{obs}}}^2} \frac{\partial C_{\ell_{\text{obs}}}^{\text{th}}}{\partial b^{\text{fid}}(k_i)} \frac{\partial C_{\ell_{\text{obs}}}^{\text{th}}}{\partial b^{\text{fid}}(k_j)}, \quad (4)$$

where  $C_{\ell_{\text{obs}}}^{\text{th}}$  is the theoretical (Eq.1)  $C_\ell$  evaluated at  $\ell = \ell_{\text{obs}}$  using the fiducial bias model  $b^{\text{fid}}(k)$  and  $\sigma_{\ell_{\text{obs}}}$  is the corresponding observational error. The data is assumed to be such that the covariance matrix is diagonal whereby only the variance  $\sigma_{\ell_{\text{obs}}}$  suffices.

The fiducial model for bias is, in principle, expected to be close to the underlying “true” model. In this work we have taken  $b^{\text{fid}}(k)$  to be the fitted polynomial obtained in the earlier section which matches the simulated bias up to an acceptable accuracy.

In the model for HI distribution at low redshifts, the mean neutral fraction crucially sets the amplitude for the power spectrum. However, a lack of precise knowledge about this quantity makes the overall amplitude of  $C_\ell$  largely uncertain. To incorporate this we have treated the quantity  $\bar{x}_{\text{HI}}$  as an additional free parameter over which the Fisher matrix is marginalized. The corresponding degraded Fisher matrix is given by

$$\mathbf{F}^{\text{deg}} = \mathbf{F} - \mathbf{B}\mathbf{F}'^{-1}\mathbf{B}^T \quad (5)$$

where  $\mathbf{F}$  is the original  $n_{\text{bin}} \times n_{\text{bin}}$  Fisher matrix corresponding to the parameters  $b_i$ ,  $\mathbf{F}'$  is a  $1 \times 1$  Fisher matrix for the additional parameter  $\bar{x}_{\text{HI}}$ , and  $\mathbf{B}$  is a  $n_{\text{bin}} \times 1$ -dimensional matrix containing the cross-terms. We shall henceforth refer to  $\mathbf{F}^{\text{deg}}$  as the Fisher matrix and implicitly assume that the marginalization has been performed.

The Fisher matrix obtained using Eq.4 and Eq.5 is illustrated in Figure 5 as a shaded plot in the  $k - k$  plane. The matrix shows a band diagonal structure with most of the information accumu-

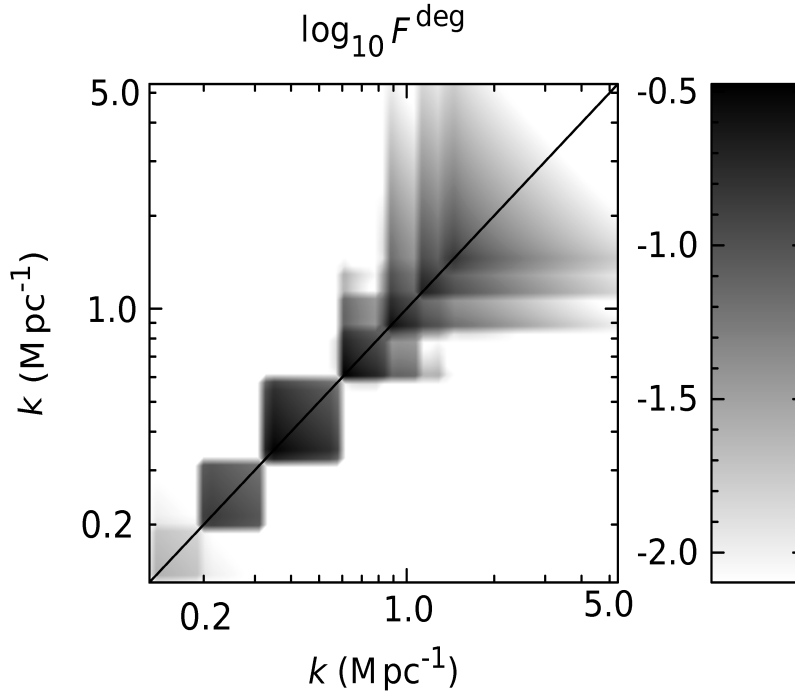


**Figure 5.** The degraded Fisher matrix  $F_{ij}^{deg}$  in the  $k-k$  plane.

lated in discrete regions especially corresponding to the  $k$ -modes for which the data is available. In the region  $k > 2$  and  $k < 0.2$   $\text{Mpc}^{-1}$ , the value of  $F_{ij}$  is relatively small, implying that one cannot constrain  $b(k)$  in those  $k$ -bins from the data set we have considered in this work.

A suitable choice of basis ensures that the parameters are not correlated. This amounts to writing the Fisher matrix in its eigen basis. Once the Fisher matrix is constructed, we determine its eigenvalues and corresponding eigenvectors. The orthonormality and completeness of the eigenfunctions, allows us to expand the deviation of  $b(k_i)$  from its fiducial model,  $\delta b_i = b(k_i) - b^{fid}(k_i)$ , as

$$\delta b_i = \sum_{p=1}^{n_{\text{bin}}} m_p S_p(k_i) \quad (6)$$

where  $S_p(k_i)$  are the principal components of  $b(k_i)$  and  $m_p$  are the suitable expansion coefficients. The advantage is that, unlike  $b(k_i)$ , the coefficients  $m_p$  are uncorrelated.

Figure 6 shows the inverse of the largest eigenvalues. Beyond the first six, all the eigenvalues are seen to be negligibly small. It is known that the largest eigenvalue corresponds to minimum variance set by the Cramer-Rao bound and vice versa. This implies that the errors in  $b(k)$  would increase drastically if modes  $i > 6$  are included. Hence, most of the relevant information is essentially contained in the first six modes with larger eigenvalues. These normalized eigenmodes are shown in the Figure 7. One can see that, all these modes almost tend to vanish for  $k > 2$  and  $k < 0.2$   $\text{Mpc}^{-1}$ , as the Fisher matrix is vanishingly small in these regions. The positions of the spikes and troughs in these modes are related to the presence of data points and their amplitudes depend on the corresponding error-bars (smaller the error, larger the amplitude).

The fiducial model adopted in our analysis may be different from the true model which dictates the data. Clearly, the recon-

struction would be poor for wide discrepancies between the two. In our analysis, the simulated bias serves as the input. In the absence of many alternative models for large scale HI bias, this serves as a reasonable fiducial model.

We assume that one can then reconstruct the function  $\delta b_i$  using only the first  $M \leq n_{\text{bin}}$  modes (see Eq. 6). Considering all the  $n_{\text{bin}}$  modes ensures that no information is thrown away. However this is achieved at the cost that errors in the recovered quantities would be very large owing to the presence of the negligibly small eigenvalues. On the contrary, lowering the number of modes can reduce the error but may introduce large biases in the recovered quantities. An important step in this analysis is therefore, to decide on the number of modes  $M$  to be used. In order to test this we consider a constant bias model to represent the true model as against the fiducial model. For a given data, figure 8 shows how the true model is reconstructed through the inclusion of more and more PCA modes. The reconstruction is directly related to the quality of the data. In the  $k$ -range where data is not available, the reconstruction is poor and the fiducial model is followed. The reconstruction is also poor for large departures of the true model from the fiducial model. We see that a reasonable reconstruction is obtained using the first 5 modes for  $k < 1$  where the data is available. In order to fix the value of  $M$ , we have used the Akaike information criterion (Liddle 2007)  $\text{AIC} = \chi_{\text{min}}^2 + 2M$ , whose smaller values are assumed to imply a more favored model. Following the strategy used by Clarkson & Zunckel (2010) and Mitra, Choudhury & Ferrara (2012), we have used different values of  $M$  (2 to 6) for which the AIC is close to its minimum and amalgamated them equally at the Monte Carlo stage when we compute the errors. In this way, we ensure that the inherent bias which exists in any particular choice of  $M$  is reduced.

We next perform the Monte-Carlo Markov Chain (MCMC) analysis over the parameter space of the optimum number of PCA

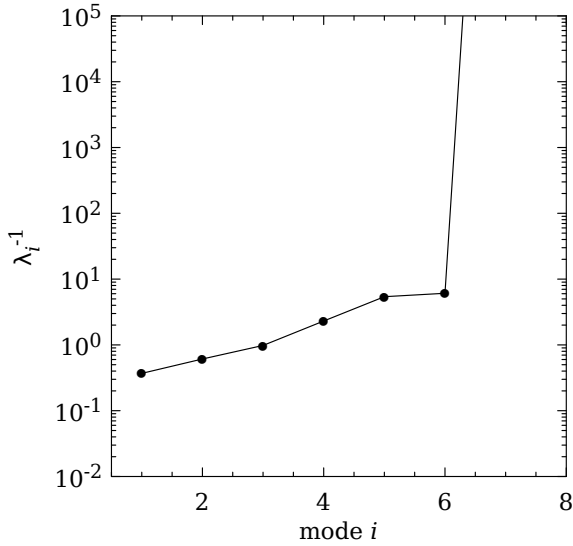


**Figure 6.** The inverse of eigenvalues of the degraded Fisher matrix  $F_{ij}^{deg}$  which essentially measures the variance on the corresponding coefficient.

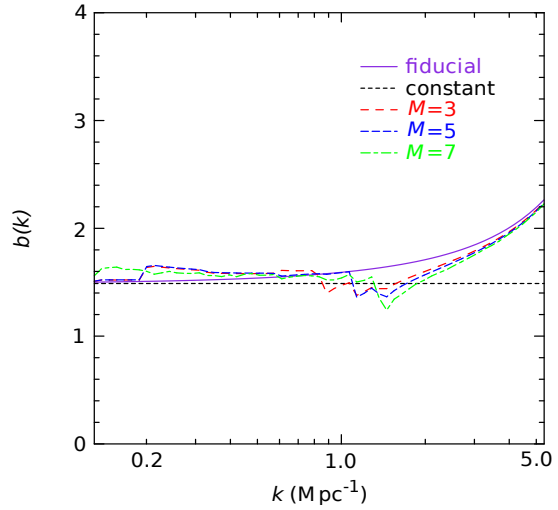


**Figure 8.** The fiducial and constant (true) bias models are shown. The reconstruction of the true model is shown for cases where number of PCA modes considered are  $M = 3, 5, 7$

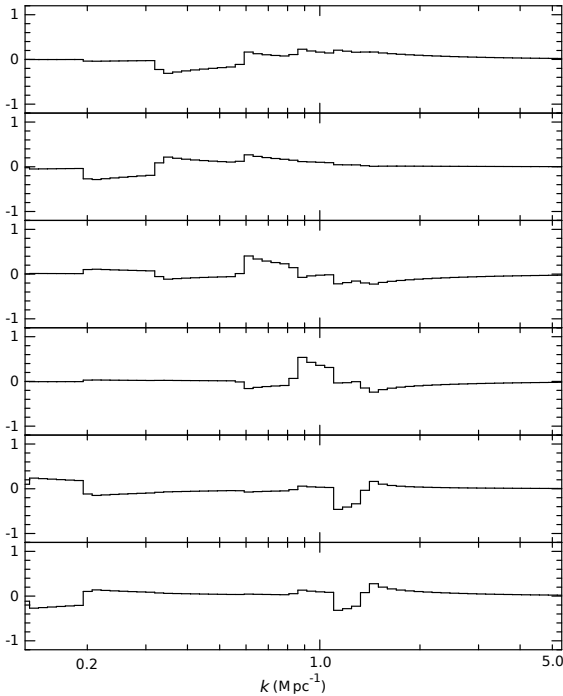


**Figure 7.** The first 6 eigenmodes of the degraded Fisher matrix.

amplitudes  $\{m_p\}$  and  $\bar{x}_{\text{HI}}$ . Other cosmological parameters are held fixed to the WMAP7 best-fit values (see Section 2). We carry out the analysis by taking  $M = 2$  to  $M = 6$  for which the AIC criterion is satisfied. By equal choice of weights for  $M$  and folding the corresponding errors together we reconstruct  $b(k)$  and thereby  $C_\ell$  along with their effective errors. We have developed a code based on the publicly available COSMOMC (Lewis & Bridle 2002) for this purpose. A number of distinct chains are run until the Gelman and Rubin convergence statistics satisfies  $R - 1 < 0.001$ . We have also used the convergence diagnostic of Raftery & Lewis to choose

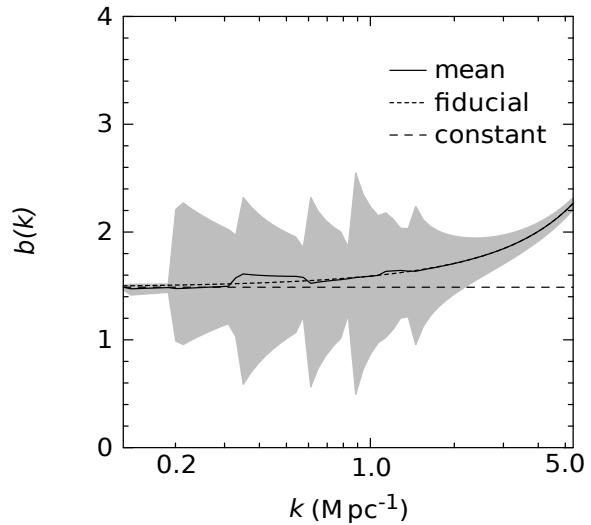


**Figure 9.** The marginalized posteriori distribution of the binned bias function obtained from the MCMC analysis using the AIC criterion up to first 6 PCA eigenmodes. The solid lines shows the mean values of bias parameters while the shaded regions represent the  $2\text{-}\sigma$  confidence limits. In addition, we show the fiducial and constant bias models.

suitable thinning conditions for each chain to obtain statistically independent samples.

## 5 RESULTS AND DISCUSSION

The reconstructed bias function obtained using the analysis described in the last section is shown in Figure 9. The solid line



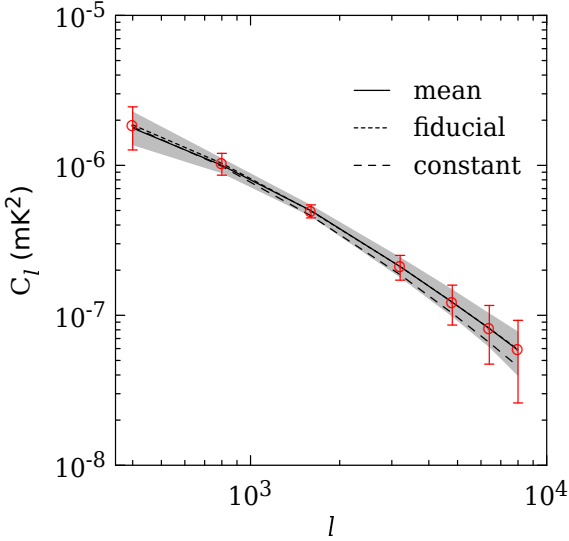


**Figure 10.** The reconstructed  $C_\ell$  with its  $2\text{-}\sigma$  confidence limits. The points with error-bars denote the observational data. The solid, short-dashed and long-dashed lines represent  $C_\ell$  for the mean, fiducial and constant bias models respectively.

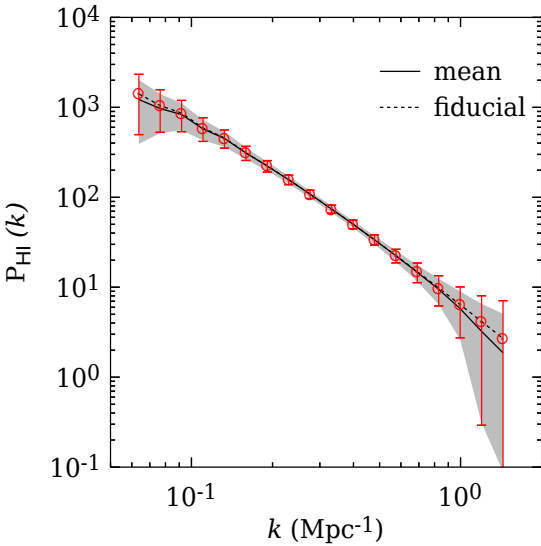


**Figure 11.** The reconstructed  $P_{\text{HI}}(k)$  with its  $2\text{-}\sigma$  confidence limits. The points with error-bars denote the observational data. We have taken  $\mu = 0.5$  and  $z = 2.5$

represents the mean model while the shaded region corresponds to  $95\%$  confidence limits ( $2\text{-}\sigma$ ). We have also shown the fiducial model (short-dashed) as well as the popularly used constant bias,  $b \sim 1.5$  model (long-dashed) for comparison. We find that the fiducial model is within the  $95\%$  confidence limits for the entire  $k$ -range considered, while the constant bias is within the same confidence limits only up to  $k \approx 2 \text{ Mpc}^{-1}$ . We note that the er-

Parameters	$2\text{-}\sigma$ errors
$\bar{x}_{\text{HI}}$	$1.06 \times 10^{-3}$
$b_{\text{lin}}$	0.453

**Table 2.** The  $2\text{-}\sigma$  errors for  $\bar{x}_{\text{HI}}$  and  $b_{\text{lin}}(k = 0.3 \text{ Mpc}^{-1})$  obtained from the current analysis using AIC criterion.

rors decrease drastically for  $k > 2$  and  $k < 0.2 \text{ Mpc}^{-1}$ . This is expected from the nature of the Fisher matrix which shows that there is practically no information in the PCA modes from these  $k$ -regions. Therefore, all models show a tendency to converge towards the fiducial one. This is a direct manifestation of lack of data points probing these scales. Thus, most of the information is concentrated in the range  $0.2 < k < 2 \text{ Mpc}^{-1}$  within which reconstruction of the bias function is relevant with the given data set.

The mean reconstructed bias simply follows the fiducial model for  $0.2 < k < 2 \text{ Mpc}^{-1}$ . This is expected as the simulated  $C_\ell$  data is generated using the fiducial bias model itself (Section 3). In the case of analysis using real observed data this matching would have statistical significance, whereas here this just serves as an internal consistency check. The shaded region depicting the errors around the mean is however meaningful and tells us how well the given data can constrain the bias. The outline of the  $2\text{-}\sigma$  confidence limits shows a jagged feature which is directly related to the presence of the data points. We observe that apart from the fiducial model, a constant bias model is also consistent with the data within the  $2\text{-}\sigma$  limits. In fact, other than imposing rough bounds  $1 \lesssim b(k) \lesssim 2$ , the present data can hardly constrain the scale-dependence of bias. It is also not possible for the  $C_\ell$  data with its error-bars to statistically distinguish between the fiducial and the constant bias model in  $0.2 < k < 2 \text{ Mpc}^{-1}$ . Figure 10 illustrates the recovered angular power spectrum with its  $95\%$  confidence limits. Superposed on it are the original data points with error-bars. We also show the angular power spectrum calculated for the fiducial and the constant bias models. The  $2\text{-}\sigma$  contour follows the pattern of the error-bars on the data points. It is evident that the data is largely insensitive (within its error-bars) to the different bias models. Hence the  $k$ -dependence of bias on these scales does not affect the observable quantity  $C_\ell$  within the bounds of statistical precision.

While constructing the Fisher matrix, we had marginalized over the largely unknown parameter  $\bar{x}_{\text{HI}}$ . Treating it as an independent free parameter, we have investigated the possibility of constraining the neutral fraction using the simulated  $C_\ell$  data. The  $2\text{-}\sigma$  error in this parameter obtained from our analysis is shown in Table 2. We had used the fiducial value  $\bar{x}_{\text{HI}} = 2.45 \times 10^{-2}$  in calculating  $C_\ell$ . It is not surprising that our analysis gives a mean  $\bar{x}_{\text{HI}} = 2.44 \times 10^{-2}$  which is in excellent agreement with the fiducial value. It is however more important to note that the given data actually constrains  $\bar{x}_{\text{HI}}$  reasonable well at  $\sim 4\%$ .

Noting that, on large scales ( $k \lesssim 0.3 \text{ Mpc}^{-1}$ ), one cannot distinguish between the mean, fiducial and the constant bias models, we use  $b_{\text{lin}} (= 1.496)$  to denote the bias value on these scales. The  $2\text{-}\sigma$  error on  $b_{\text{lin}}$  is evaluated at  $k = 0.3 \text{ Mpc}^{-1}$  (shown in Table 2).

In the  $k$ -range of our interest, the fiducial model does not reflect significant departure from the constant bias. Further, the confidence interval obtained from the data also reflects that the observed  $C_\ell$  is insensitive to the form of bias function  $b(k)$  in this range - provided that it is bound between approximate cut-offs ( $1 \lesssim b(k) \lesssim 2$ ). Moreover, the bias largely affects the amplitude of



the angular power spectrum and has only a weak contribution towards determining its shape. A scale independent large-scale bias seems to be sufficient in modelling the data. The mean neutral fraction which globally sets the amplitude of the power spectrum is hence weakly degenerate with the bias. This is manifested in the fact that though  $\bar{x}_{\text{HI}}$  is rather well constrained, the bias reconstruction which uses the degraded Fisher information (after marginalizing over  $\bar{x}_{\text{HI}}$ ) is only weakly constrained from the same data. A prior independent knowledge about the post reionization neutral fraction would clearly ensure a more statistically significant bias reconstruction with smaller errors.

Figure 11 shows the reconstructed 3D HI power spectrum. The direct algebraic relationship between the observable  $P_{\text{HI}}(k)$  and the bias  $b(k)$  makes the 3D analysis relatively straightforward. This is specifically evident since the Fisher matrix elements in this case are non-zero only along the diagonal at specific  $k$ - values corresponding to the data points. The entire routine repeated here yields similar generic features. However, the key difference is that we have a larger number of bins with high sensitivity leading to an improved constraining of bias  $1.3 < b(k) < 1.7$  in the range  $0.2 < k < 0.7 \text{ Mpc}^{-1}$ .

In the absence of real observed data, our proposed method applied on a simulated data set, reflects the possibility of constraining large-scale HI bias. The method is expected to yield better results if one has precise knowledge about the neutral content of the IGM and the underlying cosmological paradigm. We note that the problem of constraining an unknown function given a known data dealt in this work is fairly general and several alternative methods maybe used. The chief advantage of the method adopted here, apart from its effective data reduction, is its model independence. The non-parametric nature of the analysis is specially useful in the absence of any specific prior information. A straightforward fitting of a polynomial and estimating the coefficients may turn out to be effective but there is no a priori reason to believe that it would work. It is logically more reasonable not to impose a model (with its parameters) upon the data, and instead, let the data reconstruct the model.

With the anticipation of upcoming radio observations towards measurement of HI power spectrum, our method holds the promise for pinning down the nature of HI bias thereby throwing valuable light on our understanding of the HI distribution in the diffuse IGM.

## ACKNOWLEDGEMENTS

Computational work for this study was carried out at the Centre for Theoretical Studies, IIT, Kharagpur and the cluster computing facility of Harish-Chandra Research Institute<sup>4</sup>. Suman Majumdar would like acknowledge Council of Scientific and Industrial Research (CSIR), India for providing financial assistance through a Senior Research Fellowship (File No. 9/81(1099)/10-EMR-I). The authors would like to thank Prof. Somnath Bharadwaj for useful discussions and help.

## REFERENCES

Ali S. S., Bharadwaj S., Chengalur J. N., 2008, MNRAS, 385, 2166  
 Bagla J. S., Khandai N., Datta K. K., 2010, MNRAS, 407, 567  
 Becker R. H., Fan X., White R. L. e. a., 2001, ApJ, 122, 2850

Bharadwaj S., Ali S. S., 2004, MNRAS, 352, 142  
 Bharadwaj S., Ali S. S., 2005, MNRAS, 356, 1519  
 Bharadwaj S., Nath B. B., Sethi S. K., 2001, Journal of Astrophysics and Astronomy, 22, 21  
 Bharadwaj S., Sethi S. K., 2001, Journal of Astrophysics and Astronomy, 22, 293  
 Bharadwaj S., Sethi S. K., Saini T. D., 2009, PRD, 79, 083538  
 Bharadwaj S., Srikant P. S., 2004, Journal of Astrophysics and Astronomy, 25, 67  
 Chang T., Pen U., Peterson J. B., McDonald P., 2008, Physical Review Letters, 100, 091303  
 Clarkson C., Zunckel C., 2010, Physical Review Letters, 104, 211301  
 Datta K. K., Choudhury T. R., Bharadwaj S., 2007, MNRAS, 378, 119  
 Davis M., Efstathiou G., Frenk C. S., White S. D. M., 1985, ApJ, 292, 371  
 Dekel A., Lahav O., 1999, ApJ, 520, 24  
 Efstathiou G., Bond J. R., 1999, MNRAS, 304, 75  
 Eisenstein D. J., Hu W., 1998, ApJ, 496, 605  
 Fan X., Carilli C. L., Keating B., 2006, Annual Review of Astronomy & Astrophysics, 44, 415  
 Fang L., Bi H., Xiang S., Boerner G., 1993, ApJ, 413, 477  
 Furlanetto S. R., Oh S. P., Briggs F. H., 2006, Physics Report, 433, 181  
 Ghosh A., Bharadwaj S., Ali S. S., Chengalur J. N., 2010, ArXiv e-prints  
 Ghosh A., Bharadwaj S., Saiyad Ali S., Chengalur J. N., 2011, ArXiv e-prints  
 Guha Sarkar T., 2010, Journal of Cosmology and Astro-Particle Physics, 2, 2  
 Guha Sarkar T., Bharadwaj S., Choudhury T. R., Datta K. K., 2011, MNRAS, 410, 1130  
 Guha Sarkar T., Datta K. K., Bharadwaj S., 2009, Journal of Cosmology and Astro-Particle Physics, 8, 19  
 Gunn J. E., Peterson B. A., 1965, ApJ, 142, 1633  
 Haehnelt M. G., Steinmetz M., Rauch M., 2000, ApJ, 534, 594  
 Harrison E. R., 1970, PRD, 1, 2726  
 Hu W., Holder G. P., 2003, PRD, 68, 023001  
 Jarosik N., et al. 2011, The Astrophysical Journal Supplement, 192, 14  
 Jenkins A., Frenk C. S., White S. D. M., Colberg J. M., Cole S., Evrard A. E., Couchman H. M. P., Yoshida N., 2001, MNRAS, 321, 372  
 Komatsu E., et al. 2011, The Astrophysical Journal Supplement, 192, 18  
 Lanzetta K. M., Wolfe A. M., Turnshek D. A., 1995, ApJ, 440, 435  
 Leach S., 2006, MNRAS, 372, 646  
 Lewis A., Bridle S., 2002, PRD, 66, 103511  
 Liddle A. R., 2007, MNRAS, 377, L74  
 Loeb A., Wyithe J. S. B., 2008, Physical Review Letters, 100, 161301  
 Loeb A., Zaldarriaga M., 2004, Physical Review Letters, 92, 2  
 Madau P., Meiksin A., Rees M. J., 1997, ApJ, 475, 429  
 Mao Y., Tegmark M., McQuinn M., Zaldarriaga M., Zahn O., 2008, PRD, 78, 023529  
 Marín F. A., Gnedin N. Y., Seo H.-J., Vallinotto A., 2010, ApJ, 718, 972  
 McQuinn M., Zahn O., Zaldarriaga M., Hernquist L., Furlanetto S. R., 2006, ApJ, 653, 815  
 Mitra S., Choudhury T. R., Ferrara A., 2012, MNRAS, 419, 1480  
 Mitra S., Choudhury T. R., Ferrara A., 2011, MNRAS, 413, 1569  
 Mo H. J., White S. D. M., 1996, MNRAS, 282, 347  
 Pérout C., McMahon R. G., Storr-Lombardi L. J., Irwin M. J., 2003, MNRAS, 346, 1103  
 Pontzen A., Governato F., Pettini M., Booth C. M., Stinson G., Wadsley J., Brooks A., Quinn T., Haehnelt M., 2008, MNRAS, 390, 1349  
 Purcell E. M., Field G. B., 1956, ApJ, 124, 542  
 Rao S. M., Turnshek D. A., 2000, The Astrophysical Journal Supplement, 130, 1  
 Saini T. D., Bharadwaj S., Sethi S. K., 2001, ApJ, 557, 421  
 Santos M. G., Cooray A., Knox L., 2005, ApJ, 625, 575  
 Sheth R. K., Tormen G., 2002, MNRAS, 329, 61  
 Storr-Lombardi L. J., McMahon R. G., Irwin M. J., 1996, MNRAS, 283, L79  
 Visbal E., Loeb A., Wyithe S., 2009, Journal of Cosmology and Astro-Particle Physics, 10, 30

<sup>4</sup> <http://cluster.hri.res.in/index.html>

- Wolfe A. M., Gawiser E., Prochaska J. X., 2005, *Annual Review of Astronomy & Astrophysics*, 43, 861
- Wouthuysen S. A., 1952, *ApJ*, 57, 31
- Wyithe S., Brown M. J. I., 2009, *ArXiv e-prints*
- Wyithe S., Loeb A., 2007, *ArXiv e-prints*
- Wyithe S., Loeb A., 2008, *ArXiv e-prints*
- Wyithe S., Loeb A., Geil P., 2007, *ArXiv e-prints*
- Zeldovich Y. B., 1972, *MNRAS*, 160, 1P